Global Boundary Stabilization of 2D Poiseuille Flow*

Andras Balogh[a] and Miroslav Krstic[b†]
[a]Department of Mathematics, University of Texas – Pan American
Edinburg, TX 78541-2999
[b]Department of MAE, University of California at San Diego
La Jolla, CA 92093-0411

*This work was supported by grants from the Air Force Office of Scientific Research, the National Science Foundation and the Office of Naval Research.

†Author to whom correspondence should be addressed

1 Introduction

In this article we address the problem of boundary control of a viscous incompressible fluid flow in a 2D channel. Great advances have been made on this topic by Speyer and coworkers [8, 20, 21], Bewley and coworkers [4], and others employing optimal control techniques in the CFD setting. Equally impressive progress was made on the topic of controllability of Navier–Stokes equations, which is, in a sense, a prerequisite to all other problems.

Our objective in this paper is to globally *stabilize* the parabolic equilibrium profile in channel flow. This objective is different than the efforts on optimal control [2, 9, 10, 13, 15, 16, 18, 27] or controllability [6, 11, 12, 14, 17] of Navier–Stokes equations. Optimal control of nonlinear equations such as Navier–Stokes is not solvable in closed form, forcing the designer to either linearize or use computationally expensive finite–horizon model–predictive methods. Controllability–based solutions, while a prerequisite to all other problems, are not robust to changes in the initial data and model inaccuracies. The stabilization objective indirectly addresses the problems of turbulence and drag reduction, which are explicit in optimal control or controllability studies. Coron's [7] result on stabilization of Euler's equations is the first result that directly addresses flow stabilization.

The boundary feedback control we derive in this paper is fundamentally different from those in [8, 20, 21, 4], which use *wall normal* blowing and suction. Our analysis motivated by Lyapunov stabilization results in *tangential* velocity actuation. Tangential actuation is technologically feasible. The work on synthetic jets of Glezer [26] shows that a teamed up pair of synthetic jets can achieve an angle of 85° from the normal direction with the same momentum as wall normal actuation. The patent of Keefe [22] provides the means for generating tangential velocity actuation using arrays of rotating disks.

An implementational advantage in our result is that, while it uses only the measurement of wall shear stress as in the previous efforts, it employs it in a *decentralized* fashion. This means that the feedback law can be embedded into the MEMS hardware (without need for wiring).

While it is possible and important to achieve higher order $\left(H^1 \text{ and } H^2\right)$ stability, due to space limitations we restrict the analysis to the L^2 case in the present paper. For more details the interested reader is referred to [1].

The only limitation in our result is that it is guaranteed only for sufficiently low values of the Reynolds number. In simulations we demonstrate that the control law has a stabilizing effect far beyond the value required in the theorem (five or more orders of magnitude).

The paper is organized as follows. We formulate our problem in Section 2 and design boundary feedback laws in Section 3. Our main results are stated in Section 4 and L^2 stability is proved in Section 5 by employing Lyapunov techniques. In Section 6 we give numerical demonstrations that strengthen our theoretical results. Finally, in Section 7, we extend our numerical simulation to the case when the control is restricted to only part of the channel wall.

2 Problem Statement

The channel flow can be described by the 2D Navier–Stokes equations

$$\begin{cases} \mathbf{W}_t - \nu\Delta\mathbf{W} + (\mathbf{W}\cdot\nabla)\,\mathbf{W} + \nabla P = 0\,, & 0<x<1, 0<y<\ell, t>0, \\ \qquad\qquad\qquad\qquad \operatorname{div}\mathbf{W} = 0\,, & 0<x<1, 0<y<\ell, t>0, \end{cases} \tag{2.1}$$

where $\mathbf{W} = \mathbf{W}(x,y,t) = (U(x,y,t), V(x,y,t))^T$ represents the velocity vector of a particle at (x,y) and at time t, $P = P(x,y,t)$ is the pressure at (x,y) and at time t, $\nu > 0$ is the kinematic viscosity and the positive constant l represents the width of the channel. Our goal is to regulate the flow to the parabolic equilibrium profile (see Figure 1)

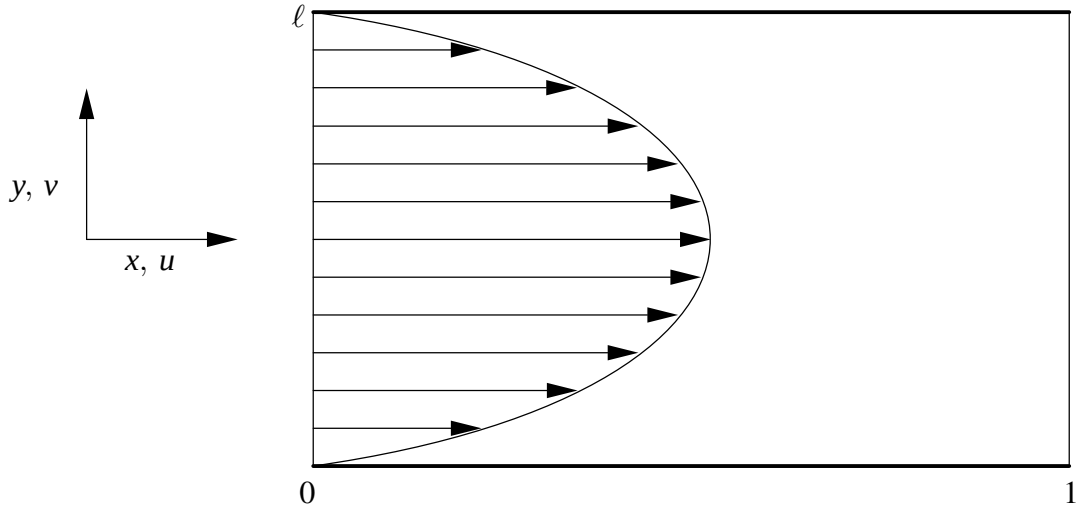

Figure 1: 2D channel flow

$$\overline{U}(y) = \frac{a}{2\nu} y(\ell - y)\,, \tag{2.2}$$

$$\overline{V} = 0\,, \tag{2.3}$$

$$\overline{P}(x) = -ax + b\,, \tag{2.4}$$

where $a = \overline{P}(0) - \overline{P}(1) \geq 0$ and $b = \overline{P}(0) \geq 0$ are constants. This profile is obtained as a fixed point of system (2.1).

To motivative our problem, let us consider the vorticity

$$\omega(x,y,t) = U_y(x,y,t) - V_x(x,y,t)\,. \tag{2.5}$$

With (2.2) and (2.3), we get the equilibrium vorticity as

$$\overline{\omega}(y) = \overline{U}'(y) - \overline{V}' = \frac{a}{2\nu}(\ell - 2y)\,. \tag{2.6}$$

Suppose the vorticity at the walls is kept at its equilibrium values

$$\omega(x,0,t) = \overline{\omega}(0)\,, \quad \omega(x,\ell,t) = \overline{\omega}(\ell)\,, \tag{2.7}$$

and the wall–normal component of the velocity at the walls is zero:

$$V(x,0,t) = 0\,, \quad V(x,\ell,t) = 0\,. \tag{2.8}$$

The objective of these no–feedback boundary conditions might be the reduction of near–wall vorticity fluctuations. These boundary conditions imply

$$U_y(x,0,t) = \omega(x,0,t) + V_x(x,0,t) = \frac{a\ell}{2\nu}\,, \tag{2.9}$$

$$U_y(x,\ell,t) = \omega(x,\ell,t) + V_x(x,\ell,t) = -\frac{a\ell}{2\nu}\,. \tag{2.10}$$

Under the boundary conditions (2.8)–(2.10), the Stokes equations

$$-\nu\Delta\mathbf{W}+(\mathbf{W}\cdot\nabla)\,\mathbf{W}+\nabla P = 0\,, \tag{2.11}$$
$$\mathrm{div}\mathbf{W} = 0 \tag{2.12}$$

has a solution

$$U = \overline{U}(y)+C\,, \tag{2.13}$$
$$V = \overline{V}\,, \tag{2.14}$$
$$P = \overline{P}(x)\,, \tag{2.15}$$

with an arbitrary constant C. This shows that under the boundary control (2.8)–(2.10) our objective of regulation to the equilibrium solution (2.2)–(2.3) can not be achieved. In more precise words, this solution is not asymptotically stable, and it can at best be marginally stable (with an eigenvalue at zero). To achieve *asymptotic* stabilization, in the next section we propose a feedback law which modifies the boundary condition (2.7).

3 Boundary Feedback Laws

In order to prepare for regulating the flow to the parabolic equilibrium profile (2.2)–(2.3), we set

$$u = U-\overline{U}\,, \tag{3.1}$$
$$\mathrm{v} = V\,, \tag{3.2}$$
$$p = P-\overline{P}\,. \tag{3.3}$$

Then equation (2.1) becomes

$$\begin{cases} u_t-\nu\Delta u+uu_x+\mathrm{v}u_y+\overline{U}u_x+\overline{U}'\mathrm{v}+p_x=0\,, & 0<x<1,0<y<\ell,t>0\,,\\ \mathrm{v}_t-\nu\Delta\mathrm{v}+u\mathrm{v}_x+\mathrm{v}\mathrm{v}_y+\overline{U}\mathrm{v}_x+p_y=0\,, & 0<x<1,0<y<\ell,t>0\,,\\ u_x+\mathrm{v}_y=0\,, & 0<x<1,0<y<\ell,t>0\,,\\ u(x,y,0)=u_0,\,v(x,y,0)=v_0\,, & 0<x<1,0<y<\ell, \end{cases} \tag{3.4}$$

To avoid dealing with an infinitely long channel, we assume that u, v, v_x and p are *periodic in the x–direction*, i.e.,

$$u(0,y,t)=u(1,y,t)\,,\,\mathrm{v}(0,y,t)=\mathrm{v}(1,y,t)\,, \qquad 0<y<\ell,t>0\,, \tag{3.5}$$
$$\mathrm{v}_x(0,y,t)=\mathrm{v}_x(1,y,t)\,,\,p(0,y,t)=p(1,y,t)\,, \qquad 0<y<\ell,t>0\,. \tag{3.6}$$

Our boundary control is applied via boundary conditions

$$\begin{cases} u(x,0,t)=ku_y(x,0,t)\,, & 0<x<1,t>0\,,\\ u(x,\ell,t)=-ku_y(x,\ell,t)\,, & 0<x<1,t>0\,,\\ \mathrm{v}(x,0,t)=0\,, & 0<x<1,t>0\,,\\ \mathrm{v}(x,\ell,t)=0\,, & 0<x<1,t>0\,, \end{cases} \tag{3.7}$$

where k is a positive constant. The physical implementation of this boundary condition is

$$U(x,0,t) = k\left[U_y(x,0,t) - \frac{a\ell}{2\nu}\right], \tag{3.8}$$

$$U(x,\ell,t) = -k\left[U_y(x,\ell,t) + \frac{a\ell}{2\nu}\right], \tag{3.9}$$

$$V(x,0,t) = 0, \tag{3.10}$$

$$V(x,\ell,t) = 0. \tag{3.11}$$

This means that we are actuating the flow velocity at the wall *tangentially*. Only the sensing of the wall shear stress $U_y(x,0,t)$ and $U_y(x,\ell,t)$ (at the respective points of actuation) is needed. The action of this feedback is pictorially represented in Figure 2. The condition (3.8) and (3.9) can be also written as

$$U(x,0,t) = k[\omega(x,0,t) - \overline{\omega}(0)], \tag{3.12}$$

$$U(x,\ell,t) = -k[\omega(x,\ell,t) - \overline{\omega}(\ell)]. \tag{3.13}$$

In the next sections we shall see that this control law achieves global asymptotic stabilization, whereas, as we saw in Section 2, the control law (2.7) is not asymptotically stabilizing.

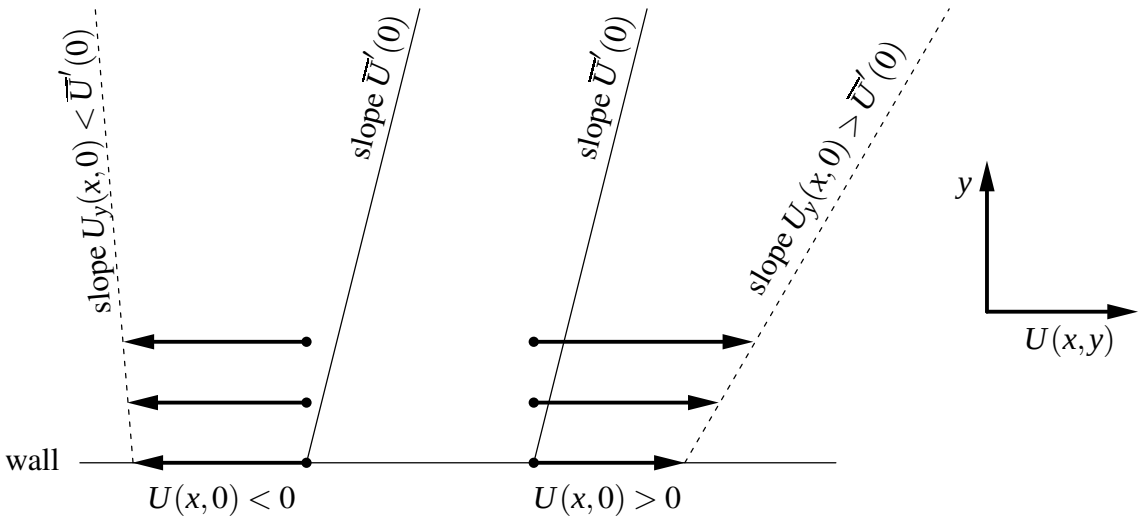

Figure 2: Tangential velocity actuation

4 The Result

Let $\Omega = (0,1) \times (0,\ell)$. In what follows, $H^s(\Omega)$ denotes the usual Sobolev space (see [24]) for any $s \in \mathbb{R}$. We shall be concerned with 2–dimensional vector function spaces and use boldface letters to denote them. For example we will use notations

$$\widetilde{\mathbf{V}} = \left\{(u,v) \in \widetilde{\mathbf{H}}^1 : u_x + v_y = 0 \text{ in } \Omega,\, v(x,0) = v(x,\ell) = 0\right\}, \tag{4.1}$$

$$\widetilde{\mathbf{H}} = \text{ the closure of } \widetilde{\mathbf{V}} \text{ in } \widetilde{\mathbf{L}}^2. \tag{4.2}$$

From now on tilde sign refers to the periodicity in the x–direction. The norm in the space $\widetilde{\mathbf{V}}$ is defined by

$$\|\mathbf{w}\|_{\widetilde{\mathbf{V}}} \;=\; ((\mathbf{w},\mathbf{w}))^{1/2}, \tag{4.3}$$

where $((\cdot,\cdot))$ denotes the inner product of $\widetilde{\mathbf{V}}$ defined by

$$((\mathbf{w},\Phi)) = \int_0^\ell \int_0^1 Tr\left\{\nabla \mathbf{w}^T \nabla \Phi\right\} dxdy + \frac{1}{k}\int_0^1 \left(u(x,0)\xi(x,0) + u(x,\ell)\xi(x,\ell)\right) dx, \tag{4.4}$$

for all $\mathbf{w} = (u,v)$, $\Phi = (\xi,\eta) \in \widetilde{\mathbf{V}}$.

Definition 4.1. *A function* $\mathbf{w} = (u,\mathrm{v}) \in L^2([0,T];\widetilde{\mathbf{V}})$ *is a* weak solution *of system (3.4)–(3.7) if*

$$\frac{d}{dt}(\mathbf{w},\Phi) + \nu((\mathbf{w},\Phi)) + ((\mathbf{w}\cdot\nabla)\mathbf{w},\Phi) + \left(\overline{U}\mathbf{w}_x,\Phi\right) + \left(\overline{U}'\mathrm{v},\xi\right) = 0 \tag{4.5}$$

is satisfied for all $\Phi = (\xi,\eta) \in \widetilde{\mathbf{V}}$ *and* $\mathbf{w}(x,y,0) = \mathbf{w}_0(x,y)$ *for all* $(x,y) \in \Omega$.

Theorem 4.1. *Suppose that*

$$\nu > \sqrt{\frac{a\ell^3}{4}} \quad \textit{and} \quad 0 < k < \ell/2, \tag{4.6}$$

and denote

$$\sigma = \frac{\nu}{\ell^2} - \frac{a\ell}{4\nu} > 0. \tag{4.7}$$

Then there exists a positive constant $c > 0$ *independent of* $\mathbf{w}_0$ *such that for the system (3.4) with periodic conditions (3.5)–(3.6), boundary control (3.7) and arbitrary initial data* $\mathbf{w}_0(x) \in \widetilde{\mathbf{H}}$, *there exists a unique weak solution* $\mathbf{w} \in L^2\left([0,\infty);\widetilde{\mathbf{V}}\right) \cap C\left([0,\infty);\widetilde{\mathbf{L}}^2\right)$ *that satisfies the global–exponential stability estimate*

$$\|\mathbf{w}(t)\| \le \|\mathbf{w}_0\| e^{-\sigma t} \qquad \textit{for all } t \ge 0. \tag{4.8}$$

Solutions depend continuously on the initial data in the L^2*–norm and the existence, uniqueness and regularity statements hold for any* $\nu > 0$ *and* $k > 0$ *over finite time intervals.*

Remark 4.1. Similar statements hold for solutions in higher order $\left(L^2\left([0,\infty);\widetilde{\mathbf{H}}^2 \cap \widetilde{\mathbf{V}}\right) \cap L^\infty\left([0,\infty);\widetilde{\mathbf{V}}\right)\right.$ and $\left. C^1\left([0,\infty);\widetilde{\mathbf{L}}^2\right) \cap C\left([0,\infty);\widetilde{\mathbf{H}}^2 \cap \widetilde{\mathbf{V}}\right)\right)$ spaces. In particular, it is possible to prove that

1. The control inputs $u(x,0,t)$ and $u(x,\ell,t)$ are bounded and go to zero as $t \to \infty$.
2. The solution $\mathbf{w}(x,y,t)$ is continuous in all three arguments. This observation has an important practical consequence: the tangential velocity actuation at nearby points on the wall will be in the same direction.

Remark 4.2. If the viscosity $\nu \le \sqrt{\frac{a\ell^3}{2}}$, the problem of boundary control remains open. The methods presented in this paper can not be applied to this case and a radically different method needs to be developed.

5 Proof of Theorem

The proof of Theorem 4.1 and the statements mentioned in Remark 4.1 goes along the lines of the classical theory of Navier–Stokes equations [23, 28] with some modifications to accommodate the nonhomogeneous boundary conditions. Lyapunov techniques and Galerkin's method are used and several technical lemmas are employed. While we refer to [1] for details, here we prove the L^2 stability estimate (4.8). This is the first step in the whole proof and it also demonstrates the use of the energy method.

Let $\mathbf{w} = (u, v)$. We define the energy $E(\mathbf{w})$ of (3.4)–(3.7) as

$$E(\mathbf{w}) = \|\mathbf{w}\|^2 = \int_0^\ell \int_0^1 \left(u^2 + v^2\right) dxdy. \tag{5.1}$$

Multiplying the first equation of (3.4) by u and the second equation of (3.4) by v and integrating over Ω by parts, we obtain

$$\begin{aligned}
\dot{E}(\mathbf{w}) &= -2\nu \int_0^\ell \int_0^1 \left(u_x^2 + u_y^2 + \mathrm{v}_x^2 + \mathrm{v}_y^2\right) dxdy - 2\int_0^\ell \int_0^1 \overline{U}' u\mathrm{v}\, dxdy \\
&\quad - \int_0^\ell u^3\big|_{x=0}^1 dy - \int_0^1 u^2\mathrm{v}\big|_{y=0}^\ell dx - \int_0^\ell \overline{U}u^2\big|_{x=0}^1 dy \\
&\quad - \int_0^\ell u\mathrm{v}^2\big|_{x=0}^1 dy - \int_0^1 \mathrm{v}^3\big|_{y=0}^\ell dx - \int_0^\ell \overline{U}\mathrm{v}^2\big|_{x=0}^1 dy \\
&\quad - 2\int_0^\ell pu|_{x=0}^1 dy - \int_0^1 p\mathrm{v}|_{y=0}^\ell dx + 2\nu \int_0^\ell u_x u|_{x=0}^1 dy \\
&\quad + 2\nu \int_0^1 u_y u\big|_{y=0}^\ell dx + 2\nu \int_0^\ell \mathrm{v}_x\mathrm{v}|_{x=0}^1 dy + 2\int_0^1 \mathrm{v}_y\mathrm{v}\big|_{y=0}^\ell dx \\
&= -2\nu \int_0^\ell \int_0^1 \left(u_x^2 + u_y^2 + \mathrm{v}_x^2 + \mathrm{v}_y^2\right) dxdy - 2\int_0^\ell \int_0^1 \overline{U}' u\mathrm{v}\, dxdy \\
&\quad + 2\nu \int_0^1 u_y u\big|_{y=0}^\ell dx.
\end{aligned} \tag{5.2}$$

Here we have used the relations

$$u_x(0,y,t) = u_x(1,y,t), \quad u_y(0,y,t) = u_y(1,y,t), \quad \text{and} \quad \mathrm{v}_y(0,y,t) = \mathrm{v}_y(1,y,t), \tag{5.3}$$

which follow from the periodic conditions (3.5)–(3.6) and the divergence free condition. Applying inequality

$$\int_0^\ell \int_0^1 \left(u^2 + \mathrm{v}^2\right) dxdy \le 2\ell \int_0^1 u^2(x,0)\, dx + \ell^2 \int_0^\ell \int_0^1 \left(u_y^2 + \mathrm{v}_y^2\right) dxdy, \tag{5.4}$$

which can be found in [1], it follows that

$$\begin{aligned}
\dot{E}(\mathbf{w}) &\leq -\frac{2\nu}{\ell^2}E(\mathbf{w}) + \frac{4\nu}{\ell}\int_0^1 u^2(x,0,t)\,dx + \frac{\ell a}{2\nu}E(\mathbf{w}) \\
&\quad -\frac{2\nu}{k}\int_0^1 \left(u^2(x,\ell,t)+u^2(x,0,t)\right)dx \\
&= -\frac{2\nu}{\ell^2}E(\mathbf{w}) + \frac{\ell a}{2\nu}E(\mathbf{w}) \\
&\quad -\int_0^1 \left(2\nu\left(\frac{1}{k}-\frac{2}{\ell}\right)u^2(x,0,t) + \frac{2\nu}{k}u^2(x,\ell,t)\right)dx \\
&\leq -\left(\frac{2\nu}{\ell^2}-\frac{a\ell}{2\nu}\right)E(\mathbf{w})\,. \qquad (5.5)
\end{aligned}$$

This implies the global–exponential stability in L^2–norm, i.e. (4.8).

Remark 5.1. The boundary integral

$$\int_0^1 \left(2\nu\left(\frac{2}{\ell}-\frac{1}{k}\right)u^2(x,0,t) - 2\nu\frac{1}{k}u^2(x,\ell,t)\right)dx \qquad (5.6)$$

in (5.5) is negative even for large Reynolds numbers (small kinematic viscosity) if k is sufficiently small. Hence, it improves the stability properties in general. The trace theorem however does not allow us to compare this term and the total energy and to prove the stability results for large Reynolds numbers. This shows the need for numerical simulation.

6 Numerical Simulation

The simulation example in this section is performed in a channel of length 4π and height 2 for Reynolds number $Re = 15000$ ($a = 2/15000$, $\nu = 1/15000$), which is five orders of magnitude greater than required in Theorem 4.1, and is three times the critical value (5772, corresponding to loss of linear stability) for 2D channel flow. The validity of the stabilization result beyond the assumptions of Theorem 4.1 is not completely surprising since our Lyapunov analysis is based on conservative energy estimates.The control gain used is $k = 1$.

A hybrid Fourier pseudospectral–finite difference discretization and the fractional step technique based on a hybrid Runge–Kutta/Crank–Nicolson time discretization was used to generate the results [3, 1, 5]. The number of grid points used in our computations was 128×120 and the (adaptive) time step was in the range of $0.05 - 0.07$. The grid points had hyperbolic tangent ($y_j = 1 + \tanh\left(s\left(2\frac{j}{NY}-1\right)\right)/\tanh(s) \quad j = 0,\ldots,NY$) distribution with stretching factor $s = 1.75$ in the vertical direction in order to achieve high resolution in the critical boundary layer. In order to obtain the flow at the walls in the controlled case the quadratic Three–Point Endpoint Formula was used to approximate the derivatives at the boundary $(U_y(x,0,t), U_y(x,\ell,t))$. This formula is applied in a semi-implicit way in order to avoid numerical instabilities. The numerical results show very good agreement with results obtained from a finite volume code used at early stages of simulations. As initial data we consider a statistically steady state flow field obtained from a random perturbation of the parabolic profile over a large time period using the uncontrolled system.

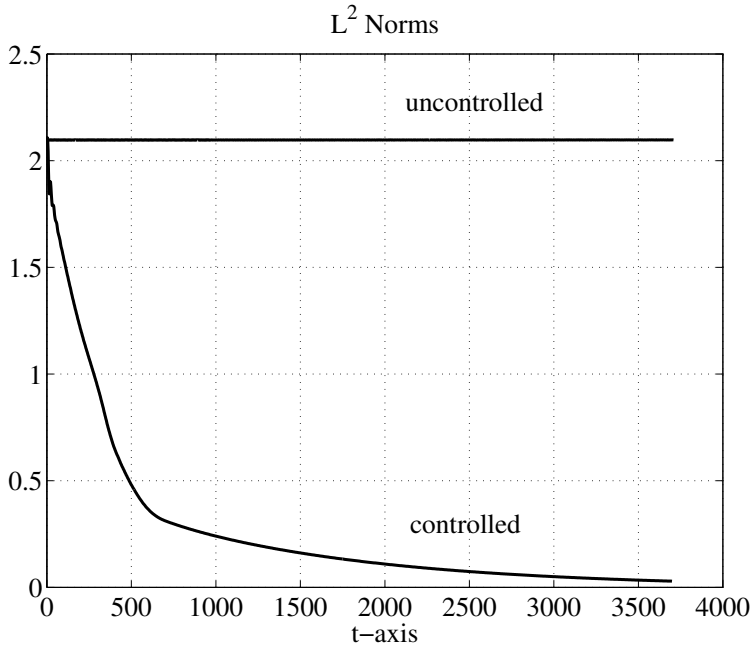

Figure 3: Energy Comparison

Figure 3 shows that our controller achieves stabilization. This is expressed in terms of the L^2–norm of the error between the steady state and the actual velocity field, the so called perturbation energy, which corresponds to system (3.4)–(3.7) with $k = 0$ (zero Dirichlet boundary conditions on the walls) in the uncontrolled case. The initially fast perturbation energy decay somewhat slows down for larger time. What we see here is an interesting example of interaction between linear and nonlinear behavior in a dynamical system. Initially, when the velocity perturbations are large, and the flow is highly nonlinear (exhibiting Tollmien–Schlichting waves with recirculation, see the uncontrolled flow in Figures 4 and 5). The strong convective (quadratic) nonlinearity dominates over the linear dynamics and the energy decay is fast. Later, at about $t = 500$, the recirculation disappears, the controlled flow becomes close to laminar, and linear behavior dominates, along with its exponential energy decay (with small decay rate).

In the vorticity map, depicted in Figure 4 it is striking how uniform the vorticity field becomes for the controlled case, while we observe quasi–periodic bursting (cf. [19]) in the uncontrolled case. We obtained similar vorticity maps of the uncontrolled flow for other (lower) Reynolds numbers, that show agreement qualitatively with the vorticity maps obtained by Jiménez [19]. His paper explains the generation of vortex blobs at the wall along with their ejection into the channel and their final dissipation by viscosity in the uncontrolled case.

The uniformity of the wall shear stress ($U_y\big|_{\text{wall}}$) in the controlled flow can be also observed in Figure 6. Our boundary feedback control (tangential actuation) adjusts the flow field near the upper boundary such that the controlled wall shear stress almost matches that of the steady state profile. The region is at the edge of a small recirculation bubble (Figure 5) of the uncontrolled flow, hence there are some flow vectors pointing in the upstream direction while others are oriented downstream. The time is relatively short ($t = 120$) after the introduction of the control and the region is small. As a result it is still possible to see actuation both downstream and upstream.

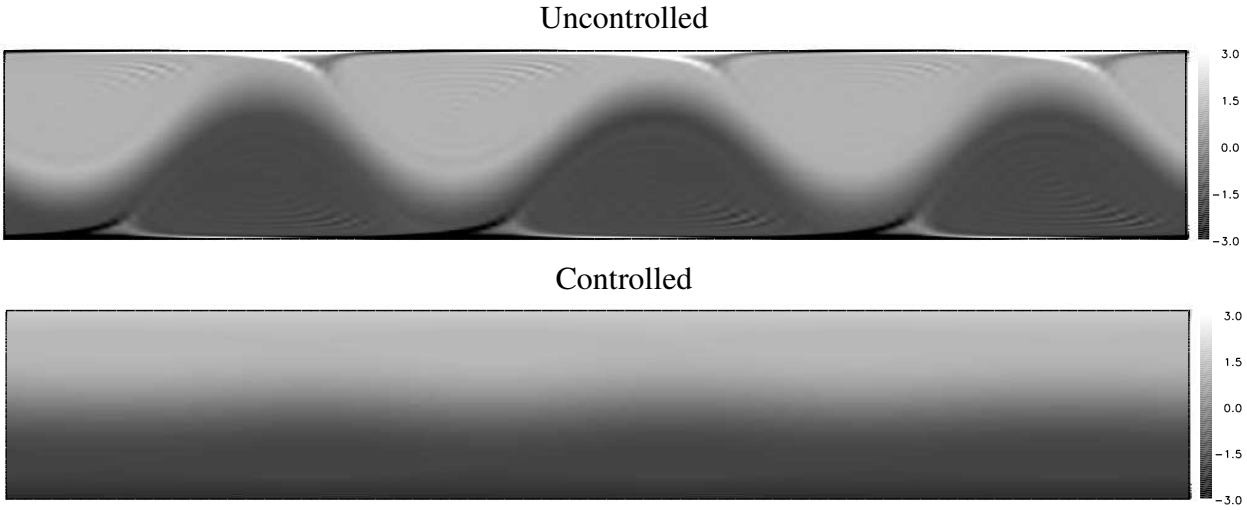

Figure 4: Vorticity Maps at $t = 700$.

Nevertheless the controlled velocity varies continuously. Figure 5 shows that the effect of control is to smear the vortical structures out in the streamwise direction. It is well known that in wall bounded turbulence instabilities are generated at the wall. In two dimensional flows these instabilities are also confined to the walls. As a result, our control effectively stabilizes the flow.

We obtain approximately 71% drag reduction (see Figure 7) as a byproduct of our special control law. The drag in the controlled case "undershoots" bellow the level corresponding to the laminar flow and eventually agrees with it up to two decimal places. It is striking that even though drag reduction was not an explicit control objective (as in most of the works in this field), the stabilization objective results in a controller that reacts to the wall shear stress error, and leads to an almost instantaneous reduction of drag to the laminar level.

7 Simulations with Only Parts of the Wall Controlled

While the use of boundary control is practically more feasible than distributed control, it is even more realistic to use control applied only on part of the boundary wall. In the present section we compare several different configurations of the channel flow with boundary control restricted to different parts of the wall (see Figure 8). The subintervals (patches) are of equal length and their number on each wall is one, two, four or eight. In addition we consider the case when control is applied only on one wall. The total length of the patches is one fourth, one third or one half of the total wall length. In all cases the control gain k introduced in (3.8) and (3.9) has been set to the value one. For these cases we present perturbation energy comparison, including the fully controlled and the uncontrolled case. Our general observations based on Figures 9 and 10 are the following.

The flow can be laminarized even when the size of the controlled region is small relative to the uncontrolled region. The smallest patch size we achieved stability with was the $1/4$ case (Figure 9, part (c)).

We achieve better performance with control concentrated in one area of the two walls than with

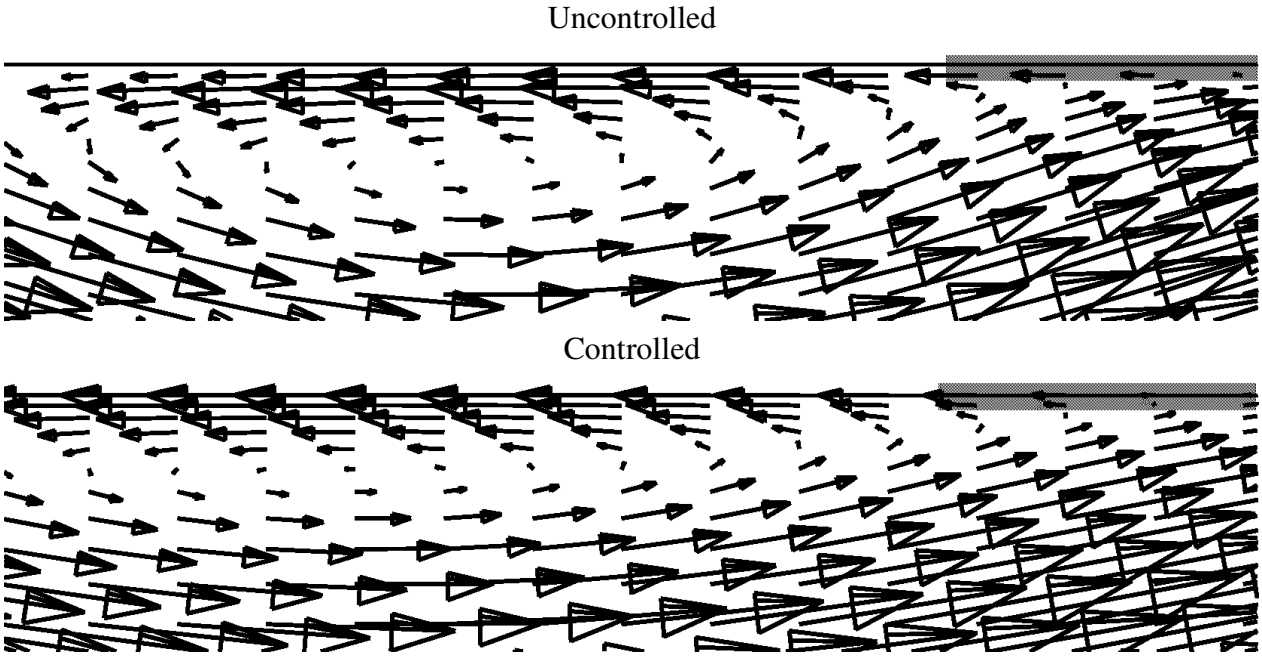

Figure 5: Recirculation in the flow at $t = 120$, in a rectangle of dimension 1.37×0.31 zoomed out of a channel of dimension $4\pi \times 2$. The shaded region (upper right corner) is magnified in Figure 6.

many small patches distributed evenly along the walls (Figure 9). With 16 patches stability was not achieved in the $1/3$ case (Figure 9, part (b)). The corresponding curve levels around the value 0.33 right after $t = 4000$. In the $1/4$ case (Figure 9, part (c)) already 8 patches degraded the control to a level where laminarization was not possible.

In the $1/2$ and $1/3$ cases concentrating all the control on one wall does not result in significantly different control performance than the one–paired configuration (Figure 9, parts (a)–(b)). In the $1/4$ case control restricted to one wall does not fully stabilize the parabolic profile, while one and two pairs of control patches do stabilize.

In a given patch configuration larger control surface achieves stability faster. The controlled and uncontrolled parts of the wall are competing against each other. The controlled part has to be large enough so that its effect has time to destroy the wall bounded turbulent structures, and the uncontrolled part has to be small enough so that instabilities do not grow over that region more than they decay over the controlled region (Figure 10).

Acknowledgment

We thank Thomas Bewley and Peter Blossey for their generous help with the numerical part of this work and continuous exchange of ideas, and we thank Javier Jiménez for his helpful comments.

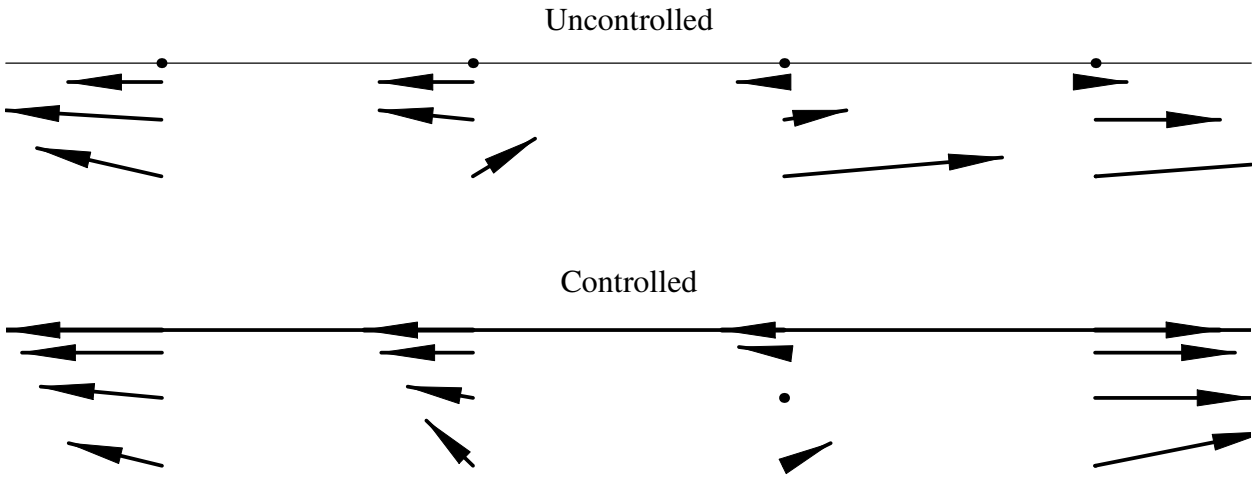

Figure 6: Velocity field in a rectangle of dimension 0.393×0.012 zoomed out of a channel of dimension $4\pi \times 2$, at time $t = 120$. The control (thick arrows) acts both *downstream* and *upstream*. The control maintains the value of shear near the desired (laminar) steady–state value.

References

[1] A. Balogh, W.-J. Liu and M. Krstic, "Stability Enhancement by Boundary Control in 2D Channel Flow," *IEEE Transactions on Automatic Control*, vol. 46, no. 11, pp. 1696–1711, 2001.

[2] V. Barbu, "The time optimal control of Navier–Stokes equations," *Systems Control Lett.,* vol. 30, no. 2–3, pp. 93–100, 1997.

[3] T.R. Bewley, P. Moin and R. Temam, "DNS–based predictive control of turbulence: an optimal benchmark for feedback algorithms," *J. Fluid Mech.,* vol. 447, pp. 179–225, 2001.

[4] T.R. Bewley, R. Temam and M. Ziane, "A general framework for robust control in fluid mechanics," *Physica D, vol.* 138, pp. 360–392, 2000.

[5] M.H. Carpenter and C.A. Kennedy, "Fourth-order 2N Runge-Kutta schemes," *NASA technical memorandum,* no. 109112, 1994.

[6] J.-M. Coron, "On the controllability of the 2–D incompressible Navier–Stokes equations with the Navier slip boundary conditions," *ESAIM: Control, Optim. Cal. Var.,* vol. 1, pp. 35–75, 1996.

[7] J.-M.Coron, On the null asymptotic stabilization of the two–dimensional incompressible Euler equations in a simply connected domain," *SIAM Journal on Control and Optimization*, vol. 37, No. 6, pp. 1874–1896, 1999.

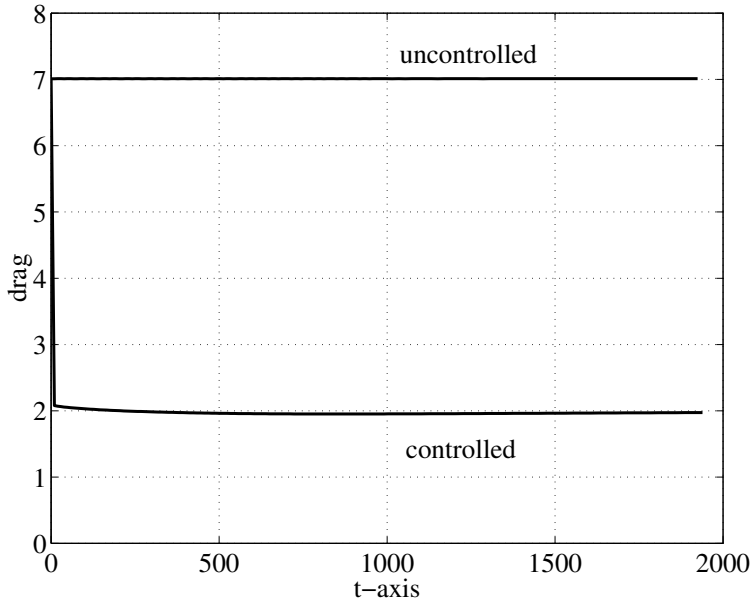

Figure 7: Instantaneous drag.

[8] L. Cortelezzi, K.H. Lee, J. Kim and J.L. Speyer, "Skin–Friction Drag Reduction Via Robust Reduced–Order Linear Feedback Control", *International Journal of Computational Fluid Dynamics*, Vol. 11, No. 1-2, 79-92, 1998.

[9] M. Desai and K. Ito, "Optimal controls of Navier–Stokes equations," *SIAM J. Control Optim.,* vol. 32, no. 5, pp. 1428–1446, 1994.

[10] H.O. Fattorini and S.S. Sritharan, "Optimal control problems with state constraints in fluid mechanics and combustion," *Appl. Math. Optim.,* vol. 38, no. 2, pp. 159–192, 1998.

[11] E. Fernández–Cara, "On the approximate and null controllability of the Navier–Stokes equations," *SIAM Rev.,* vol. 41, no. 2, pp. 269–277, 1999.

[12] A.V. Fursikov, "Exact boundary zero controllability of three–dimensional Navier–Stokes equations," *J. Dynam. Control Systems,* vol. 1, no. 3, pp. 325–350, 1995.

[13] A.V. Fursikov, M.D. Gunzburger and L.S. Hou, "Boundary value problems and optimal boundary control for the Navier–Stokes system: the two–dimensional case." *SIAM J. Control Optim.,* vol. 36, no. 3, pp. 852–894, 1998.

[14] A.V. Fursikov and O.Y. Imanuvilov, "On exact boundary zero–controllability of two–dimensional Navier–Stokes equations, Mathematical problems for Navier–Stokes equations (Centro, 1993)," *Acta Appl. Math.,* vol. 37, no. 1–2, pp. 67–76, 1994.

[15] M.D. Gunzburger, L.S. Hou, T.P. Svobodny, "Boundary velocity control of incompressible flow with an application to viscous drag reduction," *SIAM J. Control Optim.,* vol. 30, no. 1, pp. 167–181, 1992.

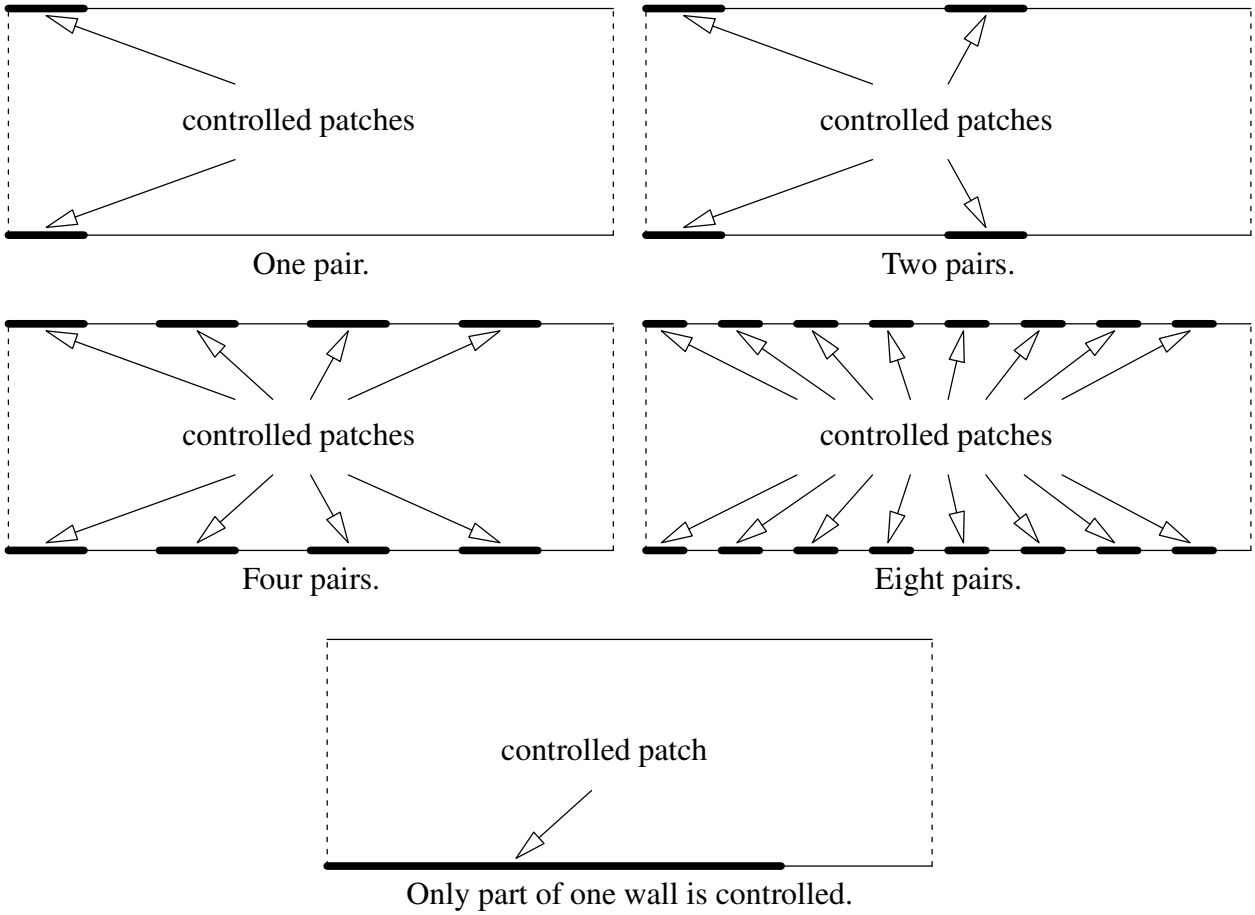

Figure 8: Configuration of control patches.

[16] L.S Hou and Y. Yan, "Dynamics and approximations of a velocity tracking problem for the Navier–Stokes flows with piecewise distributed control," *SIAM J. Control Optim.,* vol. 35, no. 6, pp. 1847–1885, 1997 .

[17] O.Y. Imanuvilov, "On exact controllability for the Navier–Stokes equations," *ESAIM: Control, Optim. Cal. Var.*, vol. 3, pp. 97–131, 1998.

[18] K. Ito and S. Kang, "A dissipative feedback control synthesis for systems arising in fluid dynamics," *SIAM J. Control Optim.,* vol. 32, no. 3, pp. 831–854, 1994.

[19] J. Jiménez, "Transition to turbulence in two–dimensional Poiseuille flow," *J. Fluid Mech.,* vol. 218, pp. 265–297, 1990.

[20] S.S. Joshi, J.L. Speyer and J. Kim, "A system theory approach to the feedback stabilization of infinitesimal and finite–amplitude disturbances in plane Poiseuille flow," *Journal of Fluid Mechanics,* vol. 332, pp. 157–184, 1997.

[21] S.S. Joshi, J.L. Speyer and J. Kim, "Finite dimensional optimal control of Poiseuille flow," *Journal of Guidance, Control, and Dynamics,* vol. 22, no. 2, pp. 340–348, 1999.

[22] L.R. Keefe, "Method and apparatus for reducing the drag of flows over surfaces," US Patent US5803409, 1998.

[23] O.A. Ladyzhenskaya, *The Mathematical Theory of Viscous Incompressible Flow*, Second English edition, Gordon and Breach, Science Publisher, Inc., New York, 1969.

[24] J.L. Lions and E. Magenes, *Non–homogeneous Boundary value Problems and Applications, Vol.I,* Springer–Verlag, Berlin, Heidelberg, New York, 1972.

[25] B.L. Rozhdestvensky and I.N. Simakin, "Secondary flows in a plane channel: their relationship and comparison with turbulent flows," *J. Fluid Mech.*, vol. 147, pp. 261–289, 1984.

[26] B.L. Smith and A. Glezer, "The formation and evolution of synthetic jets," *Phys. Fluids,* vol. 10, no. 9, pp. 2281–2297, 1998.

[27] S.S. Sritharan, "Dynamic programming of the Navier–Stokes equations," *Systems Control Lett.,* vol. 16, no. 4, pp. 299–307, 1991.

[28] R. Temam, *Navier–Stokes Equations: Theory and Numerical Analysis,* Third (Revised) edition, North–Holland Publishing Company, Amsterdam, 1984.

[29] R. Temam, *Navier–Stokes Equations and Nonlinear Functional Analysis,* Second edition, SIAM, Philadelphia, 1995.

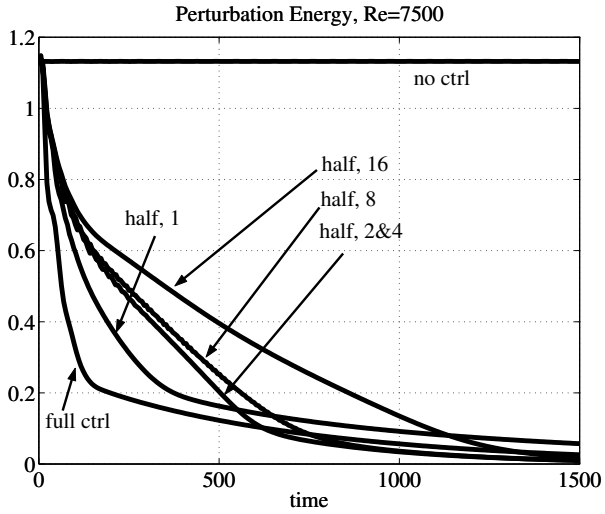

(a) Half of wall is controlled.

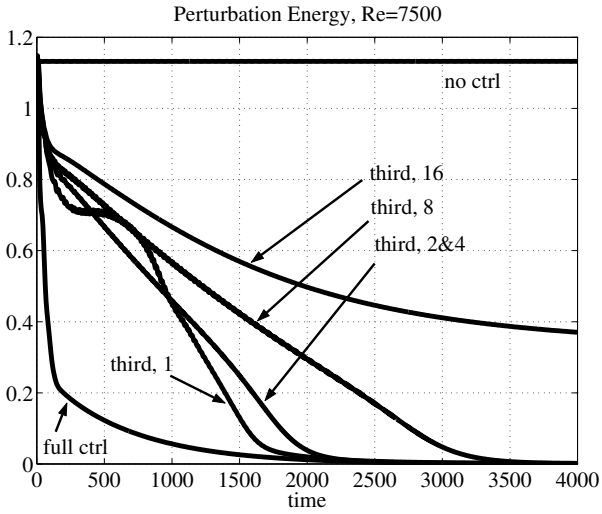

(b) Third of wall is controlled.

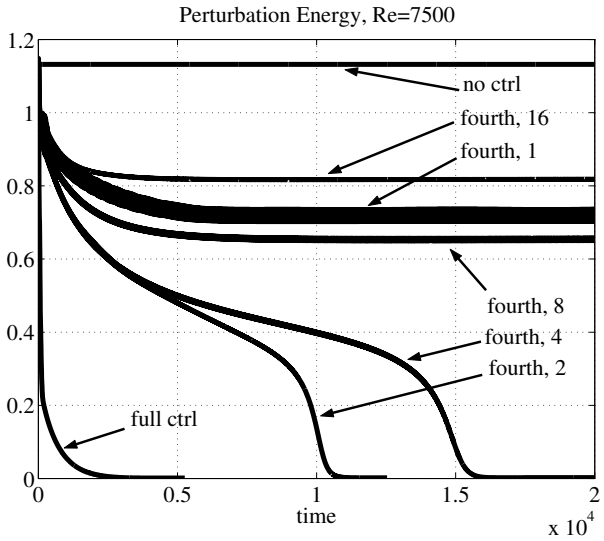

(c) Fourth of wall is controlled.

Figure 9: Comparison of perturbation energies (I).

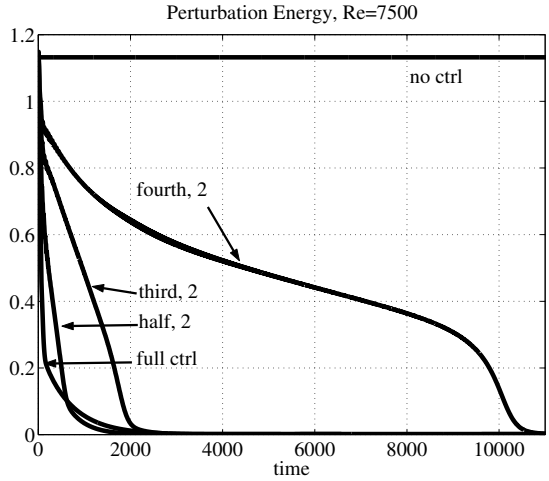

(a) One pair of patches.

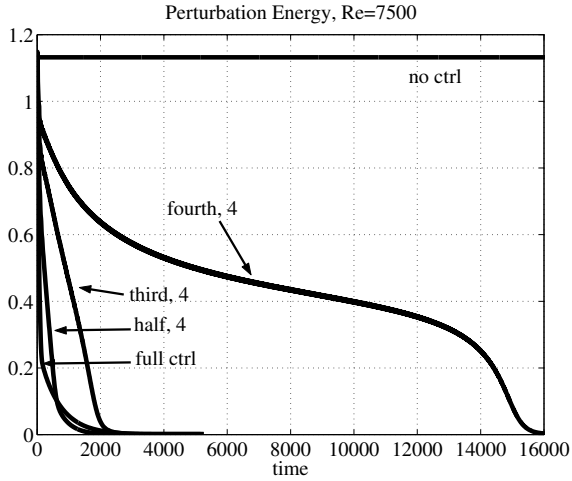

(b) Two pairs of patches.

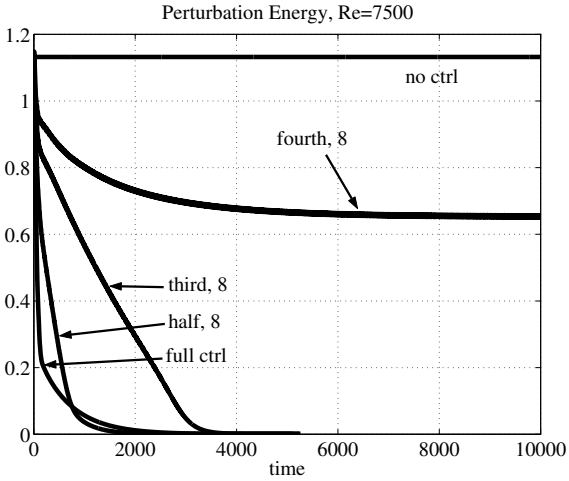

(c) Four pairs of patches.

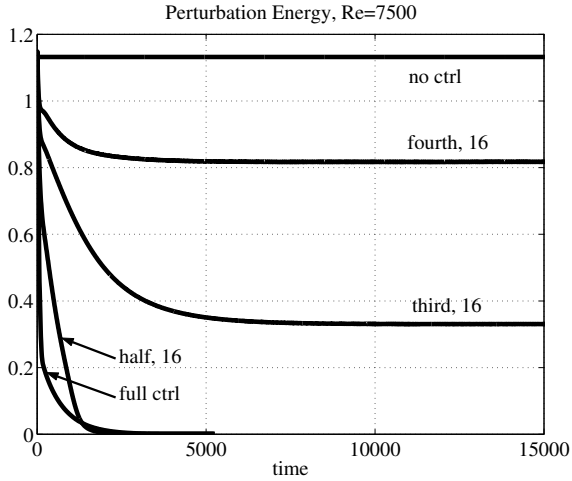

(d) Eight pairs of patches.

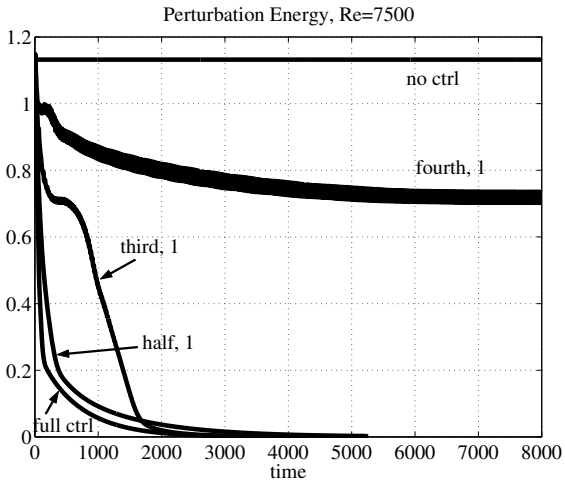

(e) One patch on bottom wall.

Figure 10: Comparisons of perturbation energies (II).